Myosin V from *Drosophila* Reveals Diversity of Motor Mechanisms within the Myosin V Family*

Judit Tóth‡§, Mihály Kovács‡, Fei Wang‡, László Nyitray§, and James R. Sellers‡¶

*From the ‡Laboratory of Molecular Physiology, NHLBI, National Institutes of Health, Bethesda, Maryland 20892-1762
and the §Department of Biochemistry, Eötvös Loránd University, Pázmány P. s. 1/c, Budapest 1117, Hungary*

Myosin V is the best characterized vesicle transporter in vertebrates, but it has been unknown as to whether all members of the myosin V family share a common, evolutionarily conserved mechanism of action. Here we show that myosin V from *Drosophila* has a strikingly different motor mechanism from that of vertebrate myosin Va, and it is a nonprocessive, ensemble motor. Our steady-state and transient kinetic measurements on single-headed constructs reveal that a single *Drosophila* myosin V molecule spends most of its mechanochemical cycle time detached from actin, therefore it has to function in processive units that comprise several molecules. Accordingly, in *in vitro* motility assays, double-headed *Drosophila* myosin V requires high surface concentrations to exhibit a continuous translocation of actin filaments. Our comparison between vertebrate and fly myosin V demonstrates that the well preserved function of myosin V motors in cytoplasmic transport can be accomplished by markedly different underlying mechanisms.

Our current understanding of the function and mechanism of vertebrate myosin V makes it the prime example of a single-molecule processive motor that walks along actin filaments to carry various cargos. Vertebrate myosin Va has been characterized extensively from many aspects including its enzymatic cycle (1–4), the regulation of its activity (5, 6), its atomic structure (7, 8), its mechanics (9, 10), and its role in cellular processes (11, 12). Other members of the myosin V family from vertebrates and yeast have been studied mainly from a cell biological point of view, and they all seem to adopt the same niche regarding their role: they participate in the short range transport and orientation of membrane particles, cellular organelles, and mRNA-protein complexes (13–17). Vertebrate myosin Va has served as the sole biochemical example so far, and it is not known how universal its mechanism of action is within the myosin V family. Although it has been shown by indirect assays that the two yeast myosin V members, Myo2p and Myo4p, may be low duty cycle motors (18) neither solution kinetic nor single molecule data are available to corroborate that hypothesis. The absence of comparative knowledge has hindered the delineation of the structural and enzymatic features that are indispensable to accomplish the tasks carried out by myosin V.

We have performed a detailed molecular characterization of recombinant *Drosophila* myosin V (DmV)[1] constructs in an attempt to shed light on the common enzymatic features of myosin V-type motors. This study is part of a multilateral approach in our laboratory to building a *Drosophila* model system for the role of myosin V. The schematic structure of a DmV molecule in Fig. 1*A* demonstrates that the structural domain architecture of DmV is identical to that of vertebrate myosin V. DmV is represented by a single heavy chain gene in *Drosophila* which does not cluster with any of the three human isoforms (Va, b, and c) in a phylogenetic analysis (Fig. 1*B*). Rather, it is a distinct entity whose evolution diverged probably from the common ancestor of vertebrate myosin V; however, we have not found any major divergence in the well conserved regions of the motor domain. The mRNA of DmV is abundant in the fly through all developmental stages, as has been reported previously (19). In cultured cells, DmV seems to participate in vesicle transport just as other myosin V does.[2]

We have studied two naturally occurring splice variants of DmV which differ only in a highly charged, 8-amino acid insert in the so-called loop 2 region (Fig. 1*C*). Loop 2 is a flexible structural element at the actin binding surface of the myosin motor domain, which is thought to be involved in actin binding through ionic interactions (20–25). Our current findings are in line with those of others in that the net charge of loop 2 alters the affinity of myosin for actin (in all nucleotide states) but does not profoundly change its kinetic pattern. From our present study, the main characteristics of the DmV ATPase cycle are (i) a rapid but energetically unfavored ATP hydrolysis step (equilibrium constant < 1); (ii) rapid product release; and (iii) low thermodynamic coupling between actin and ADP binding to DmV. These properties together make it a low duty ratio myosin (*i.e.* it spends a small fraction of its cycle time bound strongly to actin), in contrast to vertebrate myosin Va. Consistent with this, we also found in *in vitro* motility assays that double-headed DmV constructs exhibit the characteristics of low duty cycle (nonprocessive) motors that require a high myosin surface density to support movement of actin filaments.

EXPERIMENTAL PROCEDURES

Cloning, Expression, and Purification of the DmV S1 and HMM Proteins—We used the myosin V cDNA from *Drosophila melanogaster* (19) to create subfragment 1 (S1–1IQ, truncated at amino acid Gly-803), which comprises the motor domain plus one light chain binding motif.

¶ To whom correspondence should be addressed: Laboratory of Molecular Physiology, NHLBI, National Institutes of Health, 9000 Rockville Pike, Bldg. 10, Rm. 8N202, MSC 1762, Bethesda, MD 20892-1762. Tel.: 301-496-6887; Fax: 301-402-1542; E-mail: sellersj@nhlbi.nih.gov.

[1] The abbreviations used are: DmV, *Drosophila* myosin V; ATPγS, adenosine 5′-3-*O*-(thio)triphosphate; dCaM, *Drosophila* calmodulin; dmantADP and dmantATP, *N*-methylantranoyl derivatives of 2′-deoxy-ADP and ATP, respectively; HMM, heavy meromyosin-like; i-, loop 2 insertion; MDCC-PBP, *N*-[2-(1-maleimidyl)ethyl]-7-(diethylamino)coumarin-3-carboxamide-labeled phosphate-binding protein; Mlc-c, cytoplasmic myosin light chain 1; MOPS, 4-morpholinepropanesulfonic acid; S1, subfragment 1.

[2] J. Tóth, M. Kovács, F. Wang, L. Nyitray, and J. R. Sellers, unpublished data.
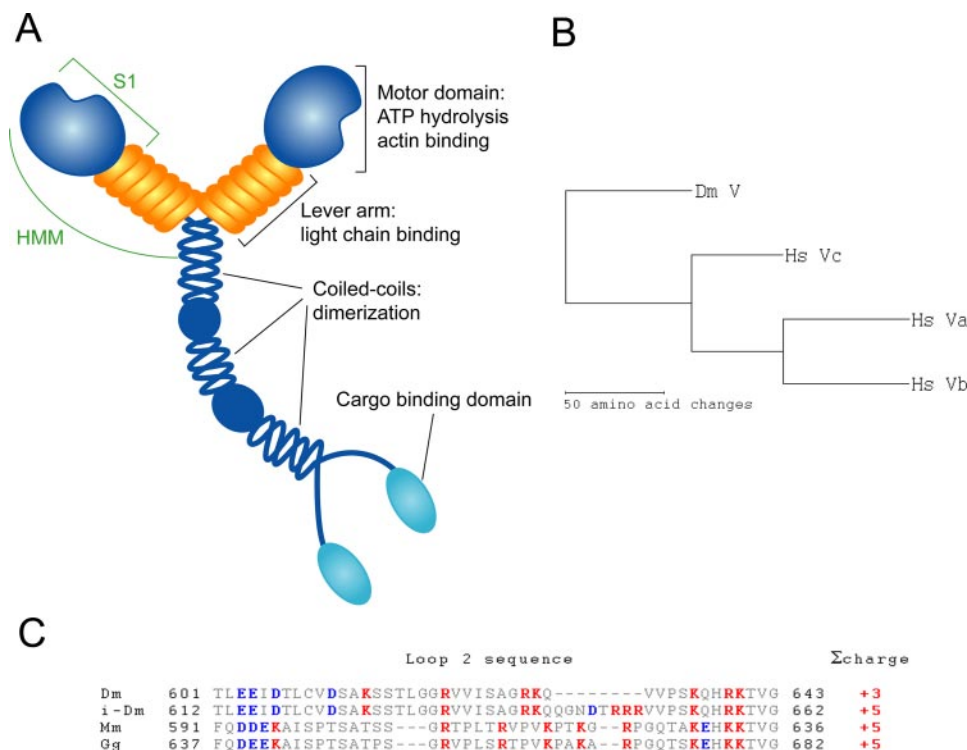
FIG. 1. *A*, schematic representation of the DmV domain structure. *Green*, recombinant protein fragments used in the experiments. *B*, phylogenetic analysis of myosin V motor domains. The consensus tree was generated from 100 bootstrapping trials by the PHYLIP package. *Dm*, *D. melanogaster*; *Hs*, *Homo sapiens*; *Va–c*, myosin isoforms. *C*, comparison of *Drosophila* and vertebrate myosin V loop 2 sequences. *Dm*, *Drosophila* myosin V; *i-Dm*, DmV with insertion in loop 2; *Mm*, mouse myosin Va; *Gg*, chicken myosin Va. Net charges of the loop 2 region are shown on the *right*. Myosin motor domain sequences were aligned by ClustalW.

We have also engineered double-headed heavy meromyosin-like (HMM) fragments that are composed of the motor and the full light chain binding domains followed by a short coiled-coil region to dimerize (truncated at amino acid Ser-1100). Fragments were subcloned into pFastbac1 (Invitrogen) baculovirus transfer vector that already contained the sequence of a FLAG tag (DYKDDDDK) downstream from the chosen cloning sites (C-terminal in the protein). We identified a splice variant of DmV bearing an 8-amino acid insert in loop 2 from expressed sequence tag data bases. We amplified and sequenced the inserted region from fly RNA. The insert (QGNDTRRR) was then introduced into the S1 and HMM sequences by QuikChange II XL mutagenesis (Stratagene) (referred to as i-S1 and i-HMM). All DNA sequences used further for protein expression have been confirmed by sequencing. All constructs were coexpressed with *Drosophila* calmodulin (dCaM) and *Drosophila* cytoplasmic myosin light chain 1 (Mlc-c). The expressed proteins were first FLAG affinity purified as described previously (26), then concentrated and fractionated on a Mono Q ion exchange column with a linear gradient of 0.1–0.5 M NaCl using ÅKTA$_{FPLC}$. Protein concentration was determined by Bradford assay using skeletal muscle S1 or HMM of known concentration in the calibration curve.

Identification of Light Chains—Small scale immune affinity purification of native myosin V from *Drosophila* was done using an affinity-purified polyclonal antibody generated against the coiled-coil region of DmV and another peptide antibody targeting the globular tail region. Mass spectrometric analysis was done on in-gel digested peptide samples of Coomassie-stained bands in the 10–20-kDa regions.

Reagents—Actin from rabbit skeletal muscle was prepared (27) and labeled with pyrene-iodoacetamide as described previously (28). ATP and ADP were of highest quality available (Roche Applied Science, 99.7% pure). *N*-Methylantranoyl derivatives of 2′-deoxy-ADP (dmantADP) and ATP (dmantATP) were generously provided by Dr. Howard White (Eastern Virginia Medical School) as well as the MDCC-labeled phosphate-binding protein (MDCC-PBP) (29). Other reagents were from Sigma.

All experiments were carried out at 25 °C in SF50 buffer unless otherwise stated. SF50 comprises 20 mM MOPS, pH 7.0, 5 mM MgCl$_2$, 50 mM KCl, 0.05 mM EGTA, 1 mM NaN$_3$ and 1 mM dithiothreitol. I = 75 mM.

Steady-state Actin-activated ATPase Measurements—ATPase activities were measured by an NADH-coupled, ATP-regenerating assay in SF50 buffer containing 1 mM ATP, 40 units/ml lactate dehydrogenase, 1 mM phosphoenolpyruvate, 200 units/ml pyruvate kinase, and 200 μM NADH. Changes in A_{340} (ϵ = 6,220 M^{-1} cm^{-1}) were followed in a Beckman DU640 spectrophotometer. The ATPase activity of actin was reduced by stabilizing the actin filaments with superstoichiometric amounts of phalloidin (Calbiochem) and was subtracted from the acto-myosin data.

Acto-S1 Cosedimentation—Phalloidin-stabilized actin filaments were mixed with S1 in SF50 buffer containing 1 mM ATP, 1 mM phosphoenolpyruvate, and 200 units/ml pyruvate kinase. Reaction mixtures were centrifuged in a Beckman TL-100 ultracentrifuge for 15 min at 100,000 rpm at 4 °C. Equal volumes of the supernatant and the resuspended pellets were run on 4–20% SDS-polyacrylamide gel. Coomassie-stained gels were digitized using a Kodak 440 Image Station, and the density data were quantified by Gaussian fits to the S1 bands to obtain the relative protein amounts.

Fluorescence Spectra—Fluorescence spectra of pyrene-labeled actin were recorded using a FluoroMax 3 (Jobin Yvon) spectrofluorometer. Excitation spectra were recorded at 406 nm emission wavelength, and emission spectra were recorded by excitation of the fluorophore at 365 nm.

In Vitro Motility Assay—The velocity of rhodamine-phalloidin-labeled actin filaments gliding over DmV HMM and i-HMM was measured as described previously (30) in a buffer comprising 20 mM MOPS, pH 7.4, 50 mM KCl, 5 mM MgCl$_2$, 1 mM ATP, 0.1 mM EGTA, 50 mM dithiothreitol, 2.5 mg/ml glucose, 2 μg/ml catalase, 0.1 mg/ml glucose oxidase, and 0.7% methylcellulose at 30 °C.

Stopped-flow Experiments—All measurements were done in an SF-2001 stopped-flow apparatus having a 2-ms dead time (KinTek Corp., Austin, TX) at 25 °C in SF50 buffer. Tryptophan fluorescence was excited at 295 nm, and emission was selected with a bandpass filter having a peak in transmittance at 347 nm. dmantATP and dmantADP were excited via energy transfer from protein tryptophans (excitation at 280 nm), the emitted light was selected using a 400 nm long pass filter. Pyrene-actin was excited at 365 nm, and its signal was monitored through a 400-nm long pass filter.

P$_i$ dissociation from the acto-S1-products complex was followed as described previously (29). MDCC-PBP was excited at 436 nm, and the emitted light was selected with a 450 nm long pass filter. Experiments were done in a double mix mode with a syringe configuration of 5 ml

(S1), 2 ml (ATP), 5 ml (actin). All syringes contained MDCC-PBP. All solutions and the stopped-flow apparatus were preincubated with a phosphate mop consisting of 0.02 unit/ml purine nucleoside phosphorylase and 0.5 mM 7-methylguanosine to eliminate P_i contamination. Only plasticware was used for buffer and protein storage. Actin filaments were stabilized with phalloidin.

Quenched-flow Experiments—Quenched-flow experiments were done as described earlier (31) except for the chemical quench being 1 M HCl instead of trichloroacetic acid.

Data Analysis and Kinetic Simulation—OriginLab 7.0 (Microcal Corp.) and the KinTek SF-2001 software were used for data fitting. We performed kinetic simulations using the Gepasi version 3.21 software (32), which is freely available on the Internet (www.gepasi.org).

RESULTS

Protein Expression and Purification—We expressed double-headed HMM and single-headed S1 constructs as well as their loop 2 inserted forms (i-HMM, i-S1). HMM comprises the N-terminal motor domain, six light chain binding motifs (IQ motifs) and a coiled-coil region to allow dimerization of the two heavy chains. S1 contains the motor domain with only one IQ motif (S1–1IQ). Proteins were expressed in the Sf9/baculovirus system at 27 °C for 3 days in shaken cultures. We could obtain >95% pure protein preparations (Fig. 2) with a heavy chain to light chain stoichiometry of ~1:1 for S1 and ~1:6 for HMM. The typical yield was 1 mg of purified protein/10^9 cells.

Light Chains Associated with DmV—*Drosophila* has at least four non-muscle myosin light chain genes (33) whose products can potentially bind to the IQ motifs of the DmV heavy chain. We raised antibodies against the tail and the coiled-coil region of DmV and used them for both immunoprecipitation and immune affinity purification of DmV from Canton S flies. Using either of the antibodies and methods we could identify Mlc-c as a binding partner for myosin V, whereas no other non-muscle

FIG. 2. **SDS-PAGE of recombinant DmV preparations.** *Lane 1*, BenchMark protein marker (Invitrogen); *lane 2*, S1–1IQ (92.5 kDa) with dCaM (17 kDa); *lane 3*, HMM (128 kDa) with dCaM and dMlc-c (16.5 kDa).

myosin light chains, including dCaM, were found (data not shown). However, when we coexpressed the HMM constructs with Mlc-c in Sf9 cells, CaM was also found associated with the purified protein (Fig. 2). This indicates that the DmV heavy chain bound endogenous CaM from the Sf9 cells and that the amount of heavy chain expression was limited by the endogenous CaM concentration of the insect cells. Thereafter we coexpressed both dCaM and Mlc-c with the heavy chain constructs. The HMM always associated with both light chains in an approximately equal stoichiometry, whereas the S1 constructs bound only dCaM (Fig. 2).

Steady-state ATPase Activity—We measured the ATPase activities of S1, i-S1, HMM, and i-HMM by an NADH-coupled assay containing an ATP-regenerating system. In both splice variants actin activated the ATPase activity ~100-fold reaching a V_{max} of 13 s^{-1} in the noninserted S1 and HMM and 15–17 s^{-1} in the i-S1 and i-HMM constructs (Fig. 3A). Half-maximal actin activation (K_{ATPase}) occurred at ~10 μM actin in the noninserted S1 and HMM at low salt concentration (I = 25 mM). Increasing the ionic strength to 75 mM by the addition of 50 mM KCl (all transient kinetic measurements were carried out in these conditions) resulted in a 2-fold increase in the K_{ATPase} of DmV S1 (19 μM). The loop 2-inserted constructs had ~4-fold reduced K_{ATPase} values compared with the noninserted ones. Steady-state parameters are compiled in Table I.

Steady-state Actin Attachment—S1 and i-S1 were sedimented with phalloidin-stabilized actin filaments in 1 mM ATP by ultracentrifugation at 4 °C. Free ADP concentration was kept to a minimum by using an ATP-regenerating system to maintain the steady-state distribution of intermediates such as in the ATPase assay. Fractional binding of S1 to actin was evaluated by densitometry after SDS-PAGE of the supernatants and pellets. Fig. 3B shows quadratic fits to the data with an apparent K_d^{app} of 5 μM for S1. The additional charges in the loop 2 of i-S1 resulted in a 5-fold increase in the steady-state S1 affinity to actin (K_d^{app} = 1 μM). The actin-bound S1 fraction represents a sum of the AM, AMT, AMDP, and AMD species in Scheme 1. Note that the experiments were carried out at 4 °C to reduce the ATPase activity of S1 to prevent depletion of ATP during the experiment.

In Vitro Motility—We used double-headed HMM and i-HMM constructs to carry out *in vitro* actin gliding motility assays. These constructs have a motor domain with six light chain binding motifs per heavy chain and a coiled-coil stalk. Therefore, the length of their lever arm (light chain binding domain) is similar to that of vertebrate myosin V. Thus, if the kinetic parameters, most relevantly the rate constant of ADP release,
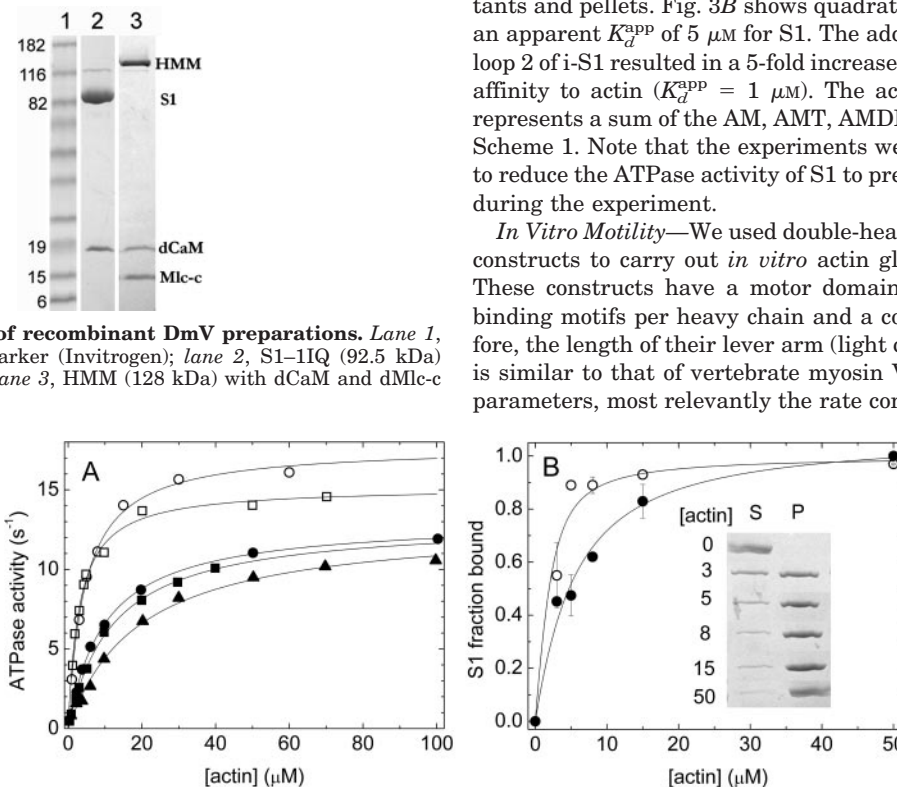

FIG. 3. **Steady-state solution properties.** *A*, actin-activated ATPase activities measured by NADH-coupled assay. *Solid circles*, S1 at 0 mM KCl (V_{max} = 13.1 s^{-1}, K_{ATPase} = 9.9 μM); *triangles*, S1 at 50 mM KCl (V_{max} = 12.9 s^{-1}, K_{ATPase} = 19.2 μM); *solid squares*, HMM (V_{max} = 13.0 s^{-1}, K_{ATPase} = 12.0 μM); *open circles*, i-S1 (V_{max} = 17.6 s^{-1}, K_{ATPase} = 4.4 μM); *open squares*, i-HMM (V_{max} = 15.2 s^{-1}, K_{ATPase} = 3.0 μM). *B*, steady-state actin attachment in 1 mM ATP was measured by actomyosin sedimentation. *Solid circles*, 2 μM S1; *open circles*, 2 μM i-S1. Acto-S1 containing pyruvate kinase and phosphoenolpyruvate was centrifuged at 4 °C, pellets were resuspended in equal volumes of buffer, and supernatants (*S*) and pellets (*P*) were run on 4–20% SDS gel. Fractional attachments were obtained by densitometry. Points are the average of two experiments, *error bars* represent the S.D. Bands shown belong to one of the experiments with S1. Actin concentrations are in μM.
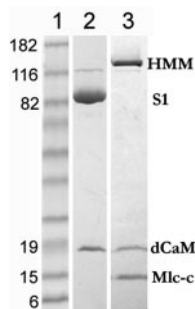
Parameter	Method	S1	i-S1	HMM	i-HMM
Motility (μm/s)	*In vitro*			0.46 ± 0.10^a 0.46 ± 0.08^b	0.65 ± 0.16^a
V_{max} (s^{-1})	NADH assay	12.5 ± 0.8^c 12.9^a	17.8 ± 0.4^a	12.6 ± 0.5^c	15.2 ± 0.27^d
K_{ATPase} (μM)	NADH assay	9.9 ± 0.6^c 19.2^a	4.3 ± 0.4^a	10.8 ± 1.2^c	3.0 ± 0.20^d
Steady-state actin binding K_d (μM)	Acto-S1 cosedimentation	$5 \pm 0.7^{a,e}$	$1 \pm 0.4^{a,e}$		

^{a} I = 75 mM.
^{b} dmantATP.
^{c} I = 25 mM.
^{d} I = 42 mM.
^{e} 4 °C.

$$AM + ATP \underset{K_1'}{\rightleftharpoons} AM(ATP) \underset{K_2'}{\rightleftharpoons} AM \cdot ATP \underset{K_3'}{\rightleftharpoons} AM \cdot ADP \cdot P_i \underset{K_4'}{\rightleftharpoons} AM \cdot ADP \underset{K_5'}{\rightleftharpoons} AM$$

$$\updownarrow K_6 \qquad \updownarrow K_7 \qquad \updownarrow K_8 \qquad \updownarrow K_9 \qquad \updownarrow K_{10} \qquad \updownarrow K_6$$

$$M + ATP \underset{K_1}{\rightleftharpoons} M(ATP) \underset{K_2}{\rightleftharpoons} M \cdot ATP \underset{K_3}{\rightleftharpoons} M \cdot ADP \cdot P_i \underset{K_4}{\rightleftharpoons} M \cdot ADP \underset{K_5}{\rightleftharpoons} M$$
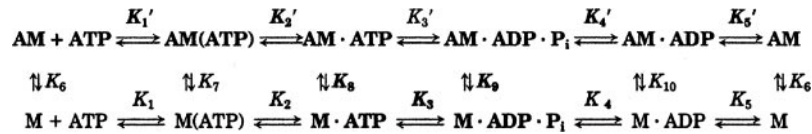
SCHEME 1

are similar in mouse myosin Va and DmV, we expect to see a similar behavior in the *in vitro* motility assay. We observed a smooth movement of actin filaments by DmV in conditions where the HMM was applied to the nitrocellulose-coated surface in a relatively high concentration (0.2–0.3 mg/ml), and 0.7% methylcellulose was present in the flow cell. Under these conditions the actin gliding velocity of HMM in 1 mM ATP was 0.46 $\pm$ 0.10 μm/s, whereas the loop 2-inserted HMM moved actin filaments somewhat faster (0.65 $\pm$ 0.16 μm/s). Velocity distributions are shown in Fig. 4, and the data are summarized in Table I. Importantly, at low HMM concentration (0.1 mg/ml or less), where the surface density of HMM is low, actin filaments did not stay attached to the myosin-coated surface. Even at high HMM surface densities the presence of the viscosity-enhancing agent methylcellulose was necessary to maintain actin filament attachment. CaM addition into the flow cell did not change either the velocity or the actin binding behavior of the HMM. On the other hand, in the presence of Ca^{2+} no directional movement could be observed presumably because of the dissociation of dCaM from the myosin neck.

We also measured the actin gliding velocity of DmV HMM with dmantATP that we used as substrate in further transient kinetic experiments. We found no difference in velocity using the fluorescent ATP analog (Table I and Fig. 4B).

ATP Binding and Hydrolysis in the Absence of Actin—DmV, as all other myosin Vs, has a tryptophan residue in the relay loop (Trp-494), which is known to be an intrinsic fluorescent sensor of the nucleotide state and the conformation of the nucleotide binding pocket (34–37). Upon mixing DmV S1 with substoichiometric ATP (single turnover conditions), a transient increase in the tryptophan fluorescence (λ_{ex} = 295 nm, λ_{em} = 347 $\pm$ 25 nm) can be observed which is followed by a slower phase with reverse amplitude (Fig. 5A). The rate constants of the initial fast phase are ATP concentration-dependent and report ATP binding to S1, whereas the second phase represents the P$_i$ release step that limits the basal ATPase cycle. The single turnover rate constant from single exponential fit to the second phase is 0.07 s^{-1}, which is in good agreement with the single turnover rates we obtained with dmantATP when performing active site titrations (data not shown). The tryptophan signal was used to determine the second order rate constant of ATP binding to S1 in pseudo-first order conditions (Fig. 5B). Time courses followed single exponentials throughout the ATP concentration range, indicating that the signal change occurred

solely between the MT and MDP states and the M → MT transition (Scheme 1) cannot be detected. Data could be fitted with a hyperbola. The maximal rate is only limited by the apparent ATP hydrolysis rate constant ($k_3 + k_{-3}$ = 68 $\pm$ 4.7 s^{-1}). The initial slope gave a second order binding rate constant of 1.31 μM^{-1} s^{-1}, which again agrees with the binding rate constants we obtained using dmantATP (data not shown).

The ATP hydrolysis step itself is reversible in all myosins ($0.6 < K_3 < 10$). We carried out single and multiple turnover quenched-flow experiments to determine whether or not DmV S1 shows evidence of a P$_i$ burst and to estimate the hydrolysis equilibrium constant (K_3) in the absence of actin. Under single turnover conditions ([ATP]/[S1] $<$ 1) the time course of the fractional hydrolysis of ATP fits to a double exponential with a small burst phase (fractional burst amplitude = 0.14) (Fig. 5C). Given that the ATP hydrolysis rate is relatively fast ($k_3 + k_{-3}$) the burst rate constant (k_{burst} = 1.86 s^{-1}) is limited by ATP binding and is close to the rate constant calculated from the ATP binding data above. The single turnover rate constant obtained from the second phase is $\sim$ 0.17 s^{-1}, which is higher and more uncertain than what we measured with other methods (Trp, dmantATP). In experiments where ATP was in 20-fold excess (Fig. 5C, *inset*) the burst phase could be clearly resolved (burst amplitude (B) = 0.4 mol of P$_i$/mol of S1) with the burst rate being the expected ATP binding rate constant (25.4 s^{-1} at 20 μM ATP). Using the equation $B = K_3/(1 + K_3)$ and the average of burst amplitudes from different experiments we calculated the hydrolysis equilibrium constant (K_3) to be 0.39 $\pm$ 0.22, which means that the hydrolysis is slightly unfavorable thermodynamically. We measured the burst on several different DmV preparations. To ensure that our quenched-flow apparatus worked well and that the small burst was not an artifact, we performed parallel control measurements with skeletal S1 as well, which yielded an expected high B of 0.95 mol P$_i$/mol S1 (data not shown).

ADP Binding and Dissociation in the Absence of Actin—Fluorescence enhancement of dmantADP upon binding to myosin was used to measure the kinetics of DmV S1 ADP binding and dissociation. Mixing of S1 with dmantADP in pseudo-first order conditions in the stopped-flow apparatus yielded single exponential time courses. The second order binding rate constant from linear least squares fit to the dmantADP concentration dependence of the observed rate constants was 2.2 $\pm$ 0.3 μM^{-1} s^{-1} (from slope), and the dissociation rate constant (y

intercept) was 37.9 ± 2.4 s^{-1} (Fig. 5D). ADP dissociation from S1 was measured by mixing the S1·dmantADP complex with 0.5 mM ATP. In these conditions the nucleotide binding site of S1 will be occupied by an ATP upon dmantADP dissociation, thus making the dissociation of the fluorescent nucleotide irreversible. Time courses followed double exponentials with a major fast phase having a $k_{obs} = 38 \pm 5.7$ s^{-1}. Note that an ADP release rate constant of ~40 s^{-1} in the absence of actin is
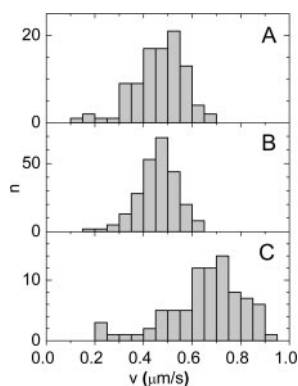

FIG. 4. **Actin gliding motility**. *A*, actin gliding velocity (*v*) distribution of DmV HMM in 1 mM ATP ($v = 0.46 \pm 0.1$ μm/s, $n = 98$); *B*, in 0.4 mM dmantATP ($v = 0.46 \pm 0.08$ μm/s, $n = 244$); *C*, i-HMM in 1 mM ATP ($v = 0.65 \pm 0.16$ μm/s, $n = 83$). Motility assays were carried out at 30 °C.

the highest among characterized myosins, although rate constants for ADP and ADP analogs can differ. The slow phase represented 15% of the total amplitude and had a k_{obs} of 4.5 s^{-1}. If it was a slow isomerization between two S1·ADP conformations we would expect a small slow phase in the binding traces as well. The binding, however, was clearly monophasic; therefore, we do not attribute a role to the slow phase in the basal ATPase mechanism.

S1-Actin Interaction—Fig. 6A shows the fluorescence excitation and emission spectra of pyrene-labeled actin alone (*a*) or saturated with DmV S1 (*b*) and skeletal muscle myosin S1 (*c*). Vertebrate myosin V quenched pyrene-actin in the same manner as skeletal S1, *i.e.* changing the relative amplitude of the 365 nm excitation peak and demonstrating a ~75% signal change when monitored at $\lambda_{em} = 406$ nm (1). DmV, however, quenches pyrene-actin only to a small extent (18% at $\lambda_{em} = 406$ nm when $\lambda_{ex} = 365$ nm), and the shape of the spectra does not change upon S1 binding to pyrene-actin. A very similar spectral behavior for myosin X has been reported recently (38). The difference in spectral changes between vertebrate and DmV upon S1 binding to pyrene-actin probably reflects differences in the design of the actomyosin interface.

We measured the rate constants of S1 and i-S1 binding to pyrene-actin with or without ADP by pseudo-first order mixing of the components in the stopped-flow. Linear fits to the k_{obs} of actin binding phases (Fig. 6B) yielded rigor binding rate constants of 2.5 μM^{-1} s^{-1} for S1 and 11.3 μM^{-1} s^{-1} for i-S1. ADP
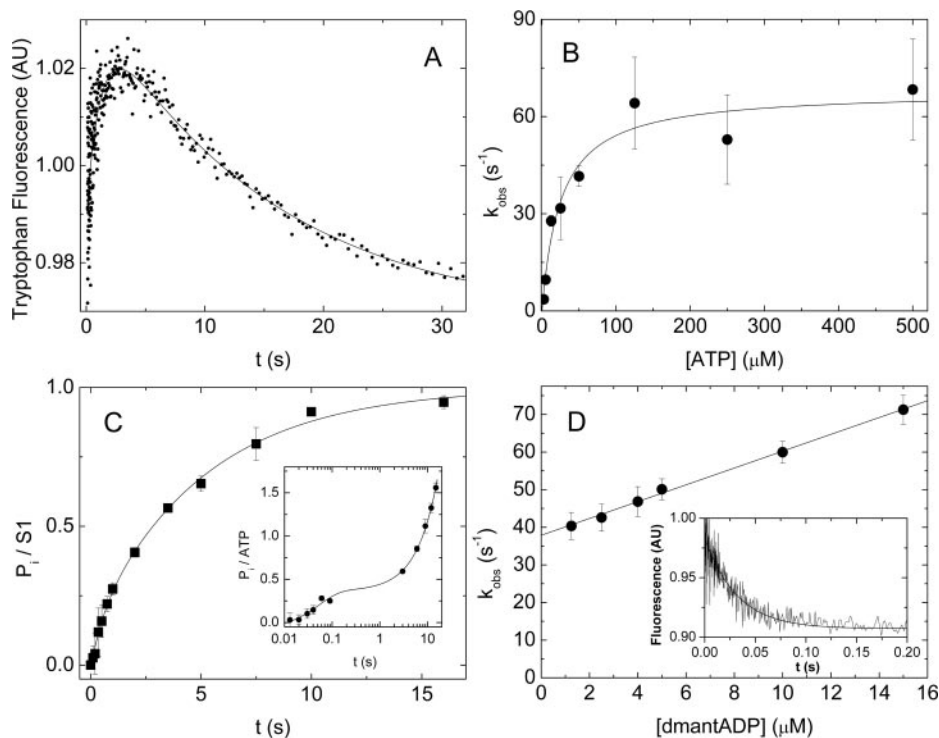

FIG. 5. **S1-nucleotide interaction.** *A*, trace of single ATP turnover as reported by the intrinsic tryptophan fluorescence signal of S1. Upon mixing 1 μM S1 with 0.5 μM ATP an ATP binding phase of increasing fluorescence and a slower phase of fluorescent decrease can be observed. A double exponential decay fits best to the data with $k_{obs} = 0.84$ s^{-1} for the binding phase and $k_{obs} = 0.066$ s^{-1} for the P$_i$ release phase. Amplitudes of the two phases are similar and report a 7% change in tryptophan fluorescence. *B*, ATP binding to S1. 0.5 μM S1 was mixed with increasing concentrations of ATP. The binding phase of the resulting tryptophan fluorescence change was fitted with single exponentials. Points are the averages of 8–10 traces. Hyperbolic fit to the data yielded a maximum rate of $k_{obs} = 68 \pm 5$ s^{-1}, which is limited by the hydrolysis step. *C*, ATP hydrolysis measured by quenched-flow. Time course of the reaction of 1 μM S1 with 0.625 μM ATP is shown. A double exponential fits best to the data and yields a burst amplitude of 0.14 mol of P$_i$/mol of S1 with a $k_{obs} = 1.9$ s^{-1} (second phase $k_{obs} = 0.2$ s^{-1}). *Inset*, ATP hydrolysis in multiple turnover conditions upon mixing 1.9 μM S1 with 20 μM ATP. Data were fit with a single exponential burst followed by a linear steady-state phase yielding a burst amplitude of 0.36 mol of P$_i$/mol of S1 with a k_{obs} of 19.2 s^{-1} and a steady-state rate of 0.08 s^{-1}. *D*, dmantADP binding to S1. dmantADP was excited by energy transfer from tryptophans near the nucleotide binding site of S1. Rate constants of the reactions of 0.25 μM S1 with different concentrations of dmantADP were obtained from single exponential fits to the averages of 8–10 traces. Linear fit to the data yielded a second order binding rate constant of 2.2 μM^{-1} s^{-1} and an intercept of 37.9 s^{-1}. *Inset*, time course on the reaction of 0.5 μM S1 and 50 μM dmantADP (premix) upon mixing with 0.5 mM ATP (postmix). A double exponential fit to this particular trace yielded a rate of 32 s^{-1} for the fast phase (85% amplitude) and 4.6 s^{-1} for the slow phase.
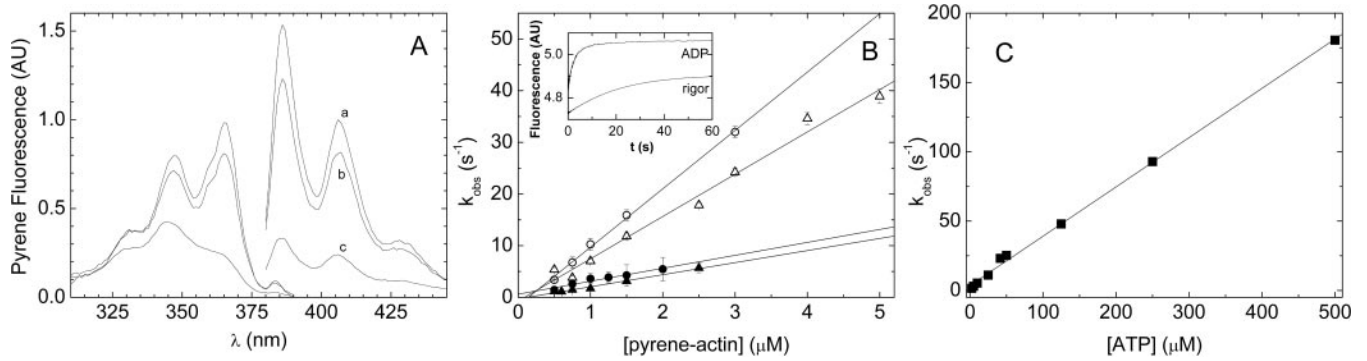
FIG. 6. **Interaction with actin.** *A*, excitation and emission spectra of pyrene-actin (*a*), pyrene-acto-DmV S1 (*b*), and pyrene-acto-S1 of skeletal myosin II (*c*). Excitation spectra were recorded at λ_{em} = 406 nm, and emission spectra were obtained by excitation at λ_{ex} = 365 nm as in all further experiments with pyrene-actin. Note the difference in the degree of quench and in the spectral profile at the λ = 365 nm excitation peak between acto-skeletal S1 and acto-DmV S1. *B*, actin binding and dissociation measured by pyrene-actin quenching. *Solid circles*, S1; *solid triangles*, S1 in ADP; *open circles*, i-S1; *open triangles*, i-S1 in ADP. Actomyosin association was measured at a constant S1:actin concentration ratio of 1:6. Stopped-flow traces were best fit to double exponentials having a concentration-dependent major slow phase and a phase of ~100 s^{-1} that did not depend on actin concentration. Rate constants shown represent the average of 12 traces. Linear fits to the data yielded the following second order association rate constants: 2.5 μM^{-1} s^{-1} for S1, 2.3 μM^{-1} s^{-1} for S1 in ADP, 11.3 μM^{-1} s^{-1} for i-S1, and 8.2 μM^{-1} s^{-1} for i-S1 in ADP. *Inset*, time courses of pyrene-acto-S1 dissociation with or without ADP present. The rigor trace resulted form the reaction of 0.15 μM pyrene- acto-S1 with 5 μM nonlabeled actin. In the ADP experiment 100 μM ADP was present is both syringes. The rigor trace fits to a single exponential and yields k_{obs} = 0.04 s^{-1}. In ADP we saw a major phase with an amplitude being 83% of the total having a k_{obs} = 0.42 s^{-1} and a minor slow phase with k_{obs} = 0.06 s^{-1}. *C*, ATP-induced pyrene-acto-S1 dissociation rates were measured by mixing 0.15 μM pyrene-acto-S1 with increasing concentrations of ATP. Single exponentials were fitted to the average of 6−8 traces to yield the k_{obs} data shown. *Error bars* are within the symbols and represent fitting error. The second order rate constant of ATP binding to pyrene-acto-S1 was 0.36 μM^{-1} s^{-1} from the slope of the linear fit to the data.

TABLE II
Transient kinetic parameters of DmV S1 and i-S1

	Parameter	Method	S1	i-S1
Single turnover	Rate constant (s^{-1})	Trp, dmantATP	0.07 ± 0.013	
		Quenched-flow	0.17 ± 0.03	
ATP binding	K_1k_2 (μM^{-1} s^{-1})	Trp, dmantATP	1.31 ± 0.52	
	$K_1'k_2'$ (μM^{-1} s^{-1})	Pyrene-actin	0.36 ± 0.006	
	$1/K_1'$ (μM)	Pyrene-actin	>500	
	k_2' (s^{-1})	$K_1'k_2'/K_1'$	>180	
ADP binding	k_{-5} (μM^{-1} s^{-1})	dmantADP	2.2 ± 0.3	
	k_5 (s^{-1})	dmantADP binding	37.9 ± 2.4	
		dmantADP chase	38.3 ± 5.7	
	K_5 (μM)	k_5/k_{-5}	17	
	k_{-5}' (μM^{-1} s^{-1})	K_5'/k_5'	4.7	4.4
	k_5' (s^{-1})	dmantADP dissociation	150	120
	K_5' (μM)	dmantADP amplitudes	32 ± 5.4	26 ± 2.0
	Coupling	K_5'/K_5	1.9	
	Acceleration	k_5'/k_5	3.9	
ATP hydrolysis	$k_3 + k_{-3}$ (s^{-1})	ATP binding (Trp)	68 ± 4.7	
	K_3	Quenched-flow	0.39 ± 0.22	
	k_3 (s^{-1})	$K_3(k_3 + k_{-3})/(1 + K_3)$	19.4	
	k_{-3} (s^{-1})	k_3/K_3	50	
	k_3' (s^{-1})	PBP double mixing	0.8 ± 0.19	
	K_3'	Simulation	~1	
Phosphate release	k_4' (s^{-1})	PBP double mixing	177 ± 18	
Actin binding	k_{-6} (μM^{-1} s^{-1})	Pyrene-actin	2.5 ± 0.29	11.3 ± 0.31
	k_6 (s^{-1})	Pyrene-actin	0.04 ± 0.001	0.009 ± 8%
	K_6 (μM)	k_{-6}/k_6	0.016	0.0008
	k_{-10} (μM^{-1} s^{-1})	Pyrene-actin	2.3 ± 0.14	8.2 ± 0.41
	k_{10} (s^{-1})	Pyrene-actin	0.43 ± 0.01	0.026 ± 4%
	K_{10} (μM)	k_{-10}/k_{10}	0.19	0.003
	K_9 (μM)	PBP double mixing	70 ± 10	

only slightly affected the actin binding rate constants (2.3 μM^{-1} s^{-1} for S1 and 8.2 μM^{-1} s^{-1} for i-S1). Time courses also had a fast phase of 90–100 s^{-1} which did not exhibit any actin concentration dependence and probably resulted from mixing artifacts. This phenomenon could not be seen in actomyosin dissociation experiments.

Pyrene-acto-S1 dissociation was measured by mixing the acto-S1 rigor complex with an excess of unlabeled actin. In the absence of nucleotide, time courses (Fig. 6*B*, *inset*) followed single exponentials with k_{obs} = 0.04 ± 0.001 s^{-1}. In 100 μM ADP, we observed a fast phase of 0.43 ± 0.011 s^{-1} (85% of total amplitude) and a slower phase of 0.057 ± 0.0022 s^{-1}. The inserted S1 behaved differently in that it exhibited two phases both with and without ADP, the slow phase being 85% of the total amplitude. (All dissociation rate constants are listed in Table II.) The calculated dissociation constant of S1 from py-
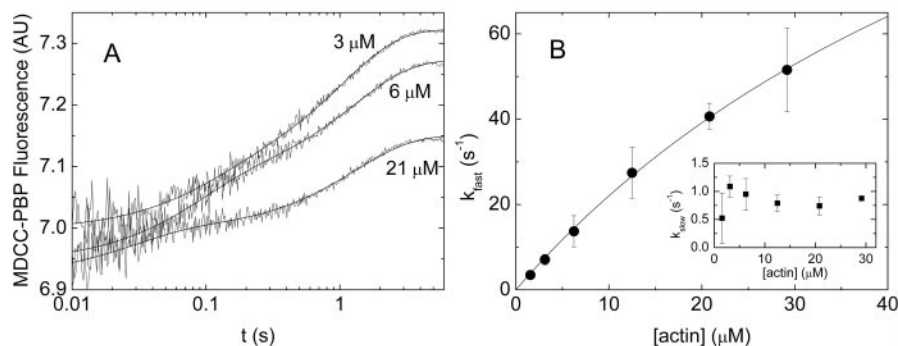
FIG. 7. **Phosphate dissociation from AMDP-products complex.** *A*, time courses of sequential mixing experiments at 3, 6, and 21 μM (postmix concentrations) actin. A fluorescent phosphate-binding protein (MDCC-PBP) was used to monitor P_i release. 3.3 μM S1 was mixed with 2 μM ATP in the first push (postmix concentration), the reaction was aged for 1 s, then was mixed with actin in 7:5 volume ratio, respectively. Smooth lines are double exponential fits to the traces. *B*, actin concentration dependence of the P_i dissociation rate constants. Data shown resulted form the analysis of 5 P_i release traces/actin concentration; *error bars* represent S.D. between them. The hyperbolic fit to k_{fast} yields a maximal rate constant of 177 ± 18 s^{-1} for P_i dissociation and $K_d = 70 \pm 10$ μM for S1·ADP·P_i binding to actin. *Inset*, the rate constants of the slow phase do not show actin concentration dependence in the examined concentration range and represent the rate constant of the ATP hydrolysis while S1 is attached to actin ($k_{slow} = 0.8 \pm 0.19$ s^{-1}).

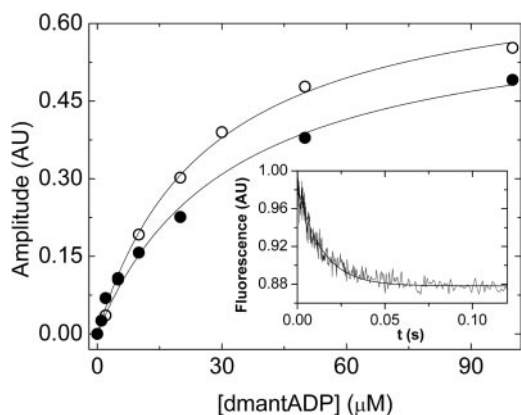FIG. 8. **ADP dissociation from actomyosin-ADP.** *Inset*, time course of the reaction on mixing 0.5 μM S1, 2 μM actin, and 20 μM dmantADP in one syringe with 1 mM ATP in the other (premix concentrations here) as reported by dmant fluorescence. Raw data were approximated with a single exponential fit yielding $k_{obs} = 71$ s^{-1}. *Main panel*, dmantADP concentration dependence of the amplitudes of single exponential fits to the ADP dissociation curves (average of 10–13 traces). *Solid circles*, S1; *open circles*, i-S1. Hyperbolic fit to the data yields an apparent dmantADP affinity of 32 μM for acto-S1 and 26 μM for acto-(i-S1). Three data points marked with *open circles* are hidden by the *solid* ones.

rene-actin (K_6) is 16 nM, which is decreased dramatically by the loop 2 insert ($K_6 = 0.8$ nM). ADP accelerates the actin dissociation from S1, thereby decreasing the affinity of S1 to actin 4 and 10-fold in i-S1 and S1, respectively, compared with rigor conditions (Table II).

ATP Binding to Actomyosin: Induction of the Weak Binding States—Binding of ATP to actomyosin induces conformational changes in the actin binding interface of myosin, which results in weakening of its actin affinity (strong-to-weak transition) and dequenching of pyrene-actin fluorescence. The weak binding myosin state then dissociates rapidly from actin, and thus the two processes (the weak-to-strong transition and dissociation) appear simultaneous. On rapid mixing of pyrene-acto-S1 with ATP in the stopped-flow, the k_{obs} of the transients will be limited by the ATP binding process at low ATP concentrations, and at high ATP concentrations it will plateau at the rate constant of the strong-to-weak isomerization. k_{obs} from single exponential fits to the time courses depended linearly on ATP concentration and did not plateau in the studied range (Fig. 6C). The slope of the linear fit yielded $K_1'k_2' = 0.36$ μM^{-1} s^{-1}.

Attached Hydrolysis and Phosphate Release—We used a fluo-

rescently labeled phosphate-binding protein (MDCC-PBP) (39) to monitor P_i dissociation from the actomyosin-products complex. In a double mixing stopped-flow experiment we first mixed S1 and ATP in single turnover conditions and allowed the ATP binding and hydrolysis to occur, then actin was mixed to the reaction to accelerate P_i dissociation. The MDCC-PBP reagent was present in all syringes in large excess over ATP. Phosphate contamination was eliminated by preincubation of all solutions with a phosphate mop (see "Experimental Procedures"). Representative single stopped-flow traces at different actin concentrations are shown in Fig. 7A. Time courses were biphasic. The slow phase had a fractional amplitude of 0.67, and its rate constant did not show actin concentration dependence within the measured range (Fig. 7B, *inset*). Following the reasoning of White *et al.* (40) we propose that the slow phase (0.8 ± 0.19 s^{-1}) reports ATP hydrolysis by myosin that is weakly bound to actin, whereas the fast phase is the actual phosphate release from the actomyosin-products complex. The observed rate constant of the fast phase is expected to exhibit a hyperbolic dependence on actin concentration which reaches its maximal velocity at saturated MDP $\leftrightarrow$ AMDP equilibrium (K_9 and k_4' in Scheme 1). Although we obtained data points only under the half-maximal saturation of this hyperbola (Fig. 7B), and therefore the maximal k_{obs} for P_i release is rather uncertain, it is clearly demonstrated that P_i release is fast and not rate-limiting in the steady-state ATPase cycle. The hyperbolic fit yielded a dissociation constant for the acto-S1-products complex (AMDP) of 70 ± 10 μM and a maximal P_i release rate constant of 177 ± 18 s^{-1}. In the second mix, actin binds to an equilibrium mixture of MT and MDP (because the hydrolysis itself is fast), therefore the fractional amplitudes of the two phases will reflect the hydrolysis equilibrium constant. Accordingly, the calculated $K_3 = 0.33 \pm 0.09$ is in good agreement with the $K_3 = 0.39 \pm 0.22$ obtained from the quenched-flow experiments.

ADP Release: Exit from the Strong Binding State—In the processive myosins V and VI so far characterized enzymatically, the apparent ADP release rate is similar to the steady-state turnover rate (1, 41, 42), therefore ADP release has been identified as a single rate-limiting step in the ATPase cycle and as a main contributor to the high duty ratio, hence the processivity of these myosins. We measured the dmantADP release from acto-S1-dmantADP by mixing it with excess unlabeled ATP. Time courses (Fig. 8, *inset*) were biphasic with a fast phase of 83 ± 18.8 s^{-1} for S1 and 70 ± 7.5 for i-S1 (average of rates obtained throughout the ADP concentration range) and a
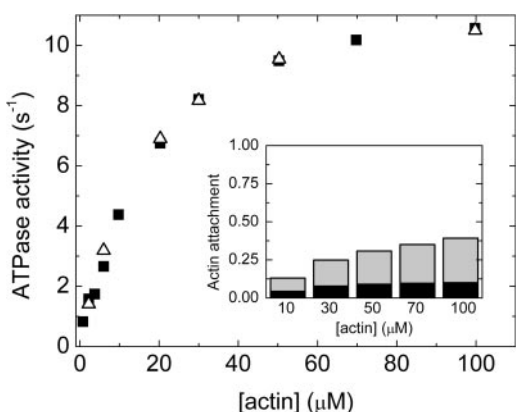
FIG. 9. **Kinetic simulation of the actomyosin ATPase cycle.** *Solid squares*, measured ATPase activities of DmV S1 in 50 mM KCl, 1 mM ATP, ATP-regenerating system at 25 °C. *Open triangles*, simulated ATPase activities using the measured transient kinetic rate constants (Table II) and the same initial concentrations as in the experiment above. Parameters k_9 and k_3' were optimized to fit the experimental data (see "Discussion"). A weak binding actin affinity of 0.5 mM for AMT was used in the simulation. *Inset*, simulation of the duty ratio (*black*) and the total actin attachment (*gray*) in steady-state using the parameters obtained from the previous global fit to the steady state ATPase activities.

minor slow phase (k_{slow} = 3.7 ± 1.21 s^{-1} for S1 and 4.3 ± 1.7 s^{-1} for i-S1). Titrations of the amplitudes (amplitude of fast phase as a function of the dmantADP concentration) yielded an apparent dmantADP affinity of 32 ± 5.4 μM for acto-S1 and 27 ± 3.2 μM for acto-i-S1 (Fig. 8). The kinetic simulation of the ADP release experiments revealed that rebinding of ADP to actomyosin at the applied ATP concentration significantly slowed the observed ADP release down proportional to the actual [ADP]:chaser [ATP] ratio. In consequence, the measured rate constants set only a lower limit to the fundamental k_5'. The simulated observed rate constants were closest to the measured ones when we set k_5' to ~ 150 s^{-1} in S1 and ~ 120 s^{-1} in i-S1. Because the observed slow rate constant seen in the experiments was much slower than the steady-state turnover rates and its fractional amplitude was constant throughout the measured ADP concentration range we surmise that it results from heterogeneity in the S1 preparation and is not part of the normal ATPase process. The calculated second order dmant-ADP binding rate constants for acto-S1 and acto-i-S1 are 4.7 and 4.4 μM^{-1} s^{-1}, respectively, implying that the insert in loop 2 does not affect the accessibility of the nucleotide binding site in an actin-bound state.

<center>DISCUSSION</center>

In this study, we show that the functional adaptation of DmV is radically different from that of vertebrate myosin V. DmV is a low duty cycle motor that must work in ensembles to achieve processivity. We have come to this conclusion after we have directly measured most of the rate constants of the ATPase cycle represented in Scheme 1 and calculated the missing interdependent parameters from these to conceptualize a plausible model for the DmV enzymatic mechanism. Furthermore, we have evaluated the motile properties of double-headed constructs and have investigated the role of excess charges conferred by a naturally occurring insertion at the actin binding interface.

Central Aspects of the DmV Enzymatic Cycle—We have determined the ATP hydrolysis equilibrium constant (K_3) by directly monitoring the hydrolysis step in chemical quench experiments. The hydrolysis equilibrium is shifted to the left, which means that breaking the chemical bond between the γ-phosphate and ADP is thermodynamically unfavorable. This phenomenon is not unique (31, 43), and the hydrolysis step is reversible in every myosin, but the shift in DmV is significant (K_3 = 0.39). The amplitude ratio of the slow and fast phases of the double mixing phosphate release experiments corroborated the value of K_3 (see "Results"). The low hydrolysis equilibrium constant allowed us to measure the rate constant of hydrolysis in an actin-attached state as well (P$_i$ dissociation experiment). This slow process is a considerable determinant of the steady-state rate at high actin concentrations where the weak binding states become more populated.

Although we have not measured it directly, P$_i$ release is probably the rate-limiting step in the basal ATPase cycle, the measured ATP binding and hydrolysis rates being both significantly faster. An interesting feature of DmV is the rapid ADP release in the absence of actin (38 s^{-1}) which may have a distinct underlying structural reason. P$_i$ dissociation is accelerated greatly (~1,700-fold) by actin, and the ADP release from AMD is also rapid (k_5' = 120–150 s^{-1}) compared with the steady-state turnover rates. The product release steps themselves therefore do not dictate the steady-state turnover rate. Another implication of the rapid product release is that both the entry to and the exit from the strong actin binding AMD state is rapid, resulting in a quick mechano-chemical cycling ("fast" myosin) with low duty ratio (nonprocessive behavior), unlike vertebrate myosin Va.

The steady-state actin activated ATPase activity of single headed DmV constructs is not limited by a single step in the cycle; rather, it is largely governed by the weak actin-binding equilibria K_3, K_9, K_3', and K_8 (Scheme 1) as it is the case in most nonprocessive myosins. The thermodynamic box defining the output of the weak binding equilibria contains experimentally inaccessible parameters such as K_8, k_{-3}', and therefore K_3'. However, using computational simulation with the measured parameters and the experimental initial nucleotide/protein concentrations as an input, we could estimate the K_8 and K_3' values that satisfy the actin concentration dependence of the steady-state rates (Fig. 9). To approximate best the experimentally determined V_{max} and K_{ATPase} at the same time, we needed to impose the combination of low affinity of myosin-ATP for actin (K_8 ~ 0.5 mM) and reversible attached hydrolysis (K_3' ~1) on the model. In that case, MT is the predominant species in steady state, and the extent of actin attachment is low (Fig. 9, *inset*). This model predicts a maximal duty ratio of 0.1 for a single head of DmV. This model does not satisfy the result of the sedimentation assay (Fig. 3B), which suggested a rather tight (K_d^{app} = 5 μM) steady-state actin attachment in the same buffer and nucleotide conditions. However, the sedimentation experiment was carried out at 4 °C instead of 25 °C because of technical difficulties in maintaining the ATP concentration at higher temperature. The fact that steady-state experiments carried out at different temperatures do not apparently satisfy the same model requirements is an indication of the vital contribution of temperature-dependent equilibria to the steady state. The hydrolysis equilibrium, or rather the previously occurring open-closed conformational transition in switch II, has been shown to be temperature-dependent in myosin II (44, 45) and in myosin V using the slowly hydrolyzable ATP analog ATPγS (3). If we hypothesize that K_3' decreases to a larger extent than K_3 at low temperature, we obtain high actin attachment. Additional temperature-dependent decreases in the ATP binding and ADP release rate constants may further increase the fraction of actin-bound heads.

Role of the Insert at the Actin Binding Interface—DmV S1 carries +3 net charges in the loop 2 region, whereas the naturally occurring splice variant i-S1 bears +5 net charges like

Motor Mechanism of Drosophila Myosin V

vertebrate myosin V (Fig. 1*C*). It has been proposed that not only the number of charged amino acids but their association into clusters is important in modulating the actin binding kinetics of myosins (25). The 8-amino acid insert in i-S1 contains a cluster of 3 arginines next to each other; therefore we expected a large effect on the actin affinity of S1. The actin binding affinities in rigor and ADP states are indeed 20–60-fold elevated, the K_{ATPase} is 4-fold lower, and the steady-state actin attachment at 4 °C is five times tighter than in the noninserted form (Tables I and II). We addressed whether the insert alters the kinetics of actomyosin ADP binding and release eventually changing the ATPase mechanism profoundly. Consistent with Yengo and Sweeney (25) we found no significant differences in the ADP kinetics. We have seen an increase, however, in the steady-state ATPase rates and in another steady-state property, the *in vitro* actin gliding velocity. These findings imply that the ADP release rate does not in itself govern either the solution or the mechanical turnover rate and that increasing the steady-state actin attachment of S1 accelerates both the ATP turnover rate and the motile speed. In conclusion, the loop 2-inserted splice variant of DmV is a somewhat faster myosin that has, nevertheless, the same kind of kinetic features as does the noninserted one. Given that the two splice variants differ only in their speed of movement, it remains a question as to whether there is any distinct role for them in the cellular processes or whether they may coexist simply because they are indistinguishable under the evolutionary pressure.

Motility—The motile speed of DmV HMM is very similar to that of mouse myosin V in an *in vitro* motility assay. In mouse myosin V, the velocity can be directly related to the step size of a myosin V having six IQ motifs (lever arm) and the rate at which myosin detaches from actin, which is practically the ADP release rate: 0.036 μm × 15 s^{-1} = 0.54 μm/s. DmV exhibits the same velocity yet having an about 10 times faster ADP release and presumably the same step size. Substituting its steady-state V_{max} in the above equation instead of its ADP release rate, however, yields the experimental velocity. Remarkably, the i-HMM that exhibits a higher V_{max} also exhibits an increased actin gliding velocity. We believe, therefore, that the same factors control both the motile speed and the solution turnover rates in DmV. Because the lifetimes of the strong binding states (AM, AMD) are short, weak binding should act instead as a drag imposed on the motile assembly (46).

Processivity—We have seen that DmV S1 has a fast ADP release and a duty ratio of 0.1 in 1 mM ATP and high actin concentration. In a double-headed molecule, the fraction of the time spent strongly bound to actin must be above 0.5 for a single head as a prerequisite for processivity. As shown before, gating between the two heads of myosin V can increase the duty ratio (10, 47, 48), but the ATPase mechanism remains basically the same in the double-headed form as it is in the single-headed one. For the double-headed DmV to be processive, the gating mechanism between the two heads should change key features of the kinetic cycle seen in S1 yet having identical steady state V_{max}, which is unlikely. In addition, DmV HMM and i-HMM do not exhibit *in vitro* motility at low surface density or in a nonviscous medium, which are typical traits of nonprocessive myosins.

Conclusion—In the present study we endeavored to explore the common enzymatic features of myosin V, and to our surprise we found profound differences between the *Drosophila* and the vertebrate members of this family. DmV displays the same steady-state rates and motile speeds as its vertebrate counterparts, but it does so by a markedly different underlying mechanism. DmV is a low duty ratio motor that would not be able to transport vesicles as a single molecule, but it can participate in organelle transport by being present in small ensembles on the surface of its cargo, thus providing processivity for its operative unit. Eventually, the role of single molecule processivity in functional adaptation to cargo transport may not be as vital as has been thought. However, high actin affinity and low thermodynamic coupling between actin and ADP binding are features that every characterized myosin involved in transport shares.

REFERENCES

1. De La Cruz, E. M., Wells, A. L., Rosenfeld, S. S., Ostap, E. M., and Sweeney, H. L. (1999) *Proc. Natl. Acad. Sci. U. S. A.* **96,** 13726–13731
2. De La Cruz, E. M., Sweeney, H. L., and Ostap, E. M. (2000) *Biophys. J.* **79,** 1524–1529
3. Yengo, C. M., De La Cruz, E. M., Safer, D., Ostap, E. M., and Sweeney, H. L. (2002) *Biochemistry* **41,** 8508–8517
4. Vale, R. D. (2003) *J. Cell Biol.* **163,** 445–450
5. Krementsov, D. N., Krementsova, E. B., and Trybus, K. M. (2004) *J. Cell Biol.* **164,** 877–886
6. Wang, F., Thirumurugan, K., Stafford, W. F., Hammer, J. A., III, Knight, P. J., and Sellers, J. R. (2004) *J. Biol. Chem.* **279,** 2333–2336
7. Coureux, P. D., Wells, A. L., Menetrey, J., Yengo, C. M., Morris, C. A., Sweeney, H. L., and Houdusse, A. (2003) *Nature* **425,** 419–423
8. Coureux, P. D., Sweeney, H. L., and Houdusse, A. (2004) *EMBO J.* **23,** 4527–4537
9. Mehta, A. D., Rock, R. S., Rief, M., Spudich, J. A., Mooseker, M. S., and Cheney, R. E. (1999) *Nature* **400,** 590–593
10. Veigel, C., Wang, F., Bartoo, M. L., Sellers, J. R., and Molloy, J. E. (2002) *Nat. Cell Biol.* **4,** 59–65
11. Cheney, R. E., O'Shea, M. K., Heuser, J. E., Coelho, M. V., Wolenski, J. S., Espreafico, E. M., Forscher, P., Larson, R. E., and Mooseker, M. S. (1993) *Cell* **75,** 13–23
12. Wu, X., Wang, F., Rao, K., Sellers, J. R., and Hammer, J. A., III (2002) *Mol. Biol. Cell* **13,** 1735–1749
13. Catlett, N. L., and Weisman, L. S. (1998) *Proc. Natl. Acad. Sci. U. S. A.* **95,** 14799–14804
14. Lapierre, L. A., Kumar, R., Hales, C. M., Navarre, J., Bhartur, S. G., Burnette, J. O., Provance, D. W., Jr., Mercer, J. A., Bahler, M., and Goldenring, J. R. (2001) *Mol. Biol. Cell* **12,** 1843–1857
15. Reck-Peterson, S. L., Provance, D. W., Jr., Mooseker, M. S., and Mercer, J. A. (2000) *Biochim. Biophys. Acta* **1496,** 36–51
16. Rodriguez, O. C., and Cheney, R. E. (2002) *J. Cell Sci.* **115,** 991–1004
17. Yin, H., Pruyne, D., Huffaker, T. C., and Bretscher, A. (2000) *Nature* **406,** 1013–1015
18. Reck-Peterson, S. L., Tyska, M. J., Novick, P. J., and Mooseker, M. S. (2001) *J. Cell Biol.* **153,** 1121–1126
19. Bonafe, N., and Sellers, J. R. (1998) *J. Muscle Res. Cell Motil.* **19,** 129–141
20. Furch, M., Geeves, M. A., and Manstein, D. J. (1998) *Biochemistry* **37,** 6317–6326
21. Joel, P. B., Trybus, K. M., and Sweeney, H. L. (2001) *J. Biol. Chem.* **276,** 2998–3003
22. Knetsch, M. L., Uyeda, T. Q., and Manstein, D. J. (1999) *J. Biol. Chem.* **274,** 20133–20138
23. Murphy, C. T., and Spudich, J. A. (1999) *Biochemistry* **38,** 3785–3792
24. Uyeda, T. Q., Ruppel, K. M., and Spudich, J. A. (1994) *Nature* **368,** 567–569
25. Yengo, C. M., and Sweeney, H. L. (2004) *Biochemistry* **43,** 2605–2612
26. Hu, A., Wang, F., and Sellers, J. R. (2002) *J. Biol. Chem.* **277,** 46512–46517
27. Spudich, J. A., and Watt, S. (1971) *J. Biol. Chem.* **246,** 4866–4871
28. Cooper, J. A., Walker, S. B., and Pollard, T. D. (1983) *J. Muscle Res. Cell Motil.* **4,** 253–262
29. Brune, M., Hunter, J. L., Corrie, J. E., and Webb, M. R. (1994) *Biochemistry* **33,** 8262–8271
30. Homsher, E., Wang, F., and Sellers, J. R. (1992) *Am. J. Physiol.* **262,** C714–C723
31. Wang, F., Kovacs, M., Hu, A., Limouze, J., Harvey, E. V., and Sellers, J. R. (2003) *J. Biol. Chem.* **278,** 27439–27448
32. Mendes, P. (1997) *Trends Biochem. Sci.* **22,** 361–363
33. Yamashita, R. A., Sellers, J. R., and Anderson, J. B. (2000) *J. Muscle Res. Cell Motil.* **21,** 491–505
34. Batra, R., and Manstein, D. J. (1999) *Biol. Chem.* **380,** 1017–1023
35. Malnasi-Csizmadia, A., Woolley, R. J., and Bagshaw, C. R. (2000) *Biochemistry* **39,** 16135–16146
36. Park, S., and Burghardt, T. P. (2000) *Biochemistry* **39,** 11732–11741
37. Yengo, C. M., Chrin, L. R., Rovner, A. S., and Berger, C. L. (2000) *J. Biol. Chem.* **275,** 25481–25487
38. Kovacs, M., Wang, F., and Sellers, J. R. (2005) *J. Biol. Chem.* **280,** 15071–15083
39. Brune, M., Corrie, J. E., and Webb, M. R. (2001) *Biochemistry* **40,** 5087–5094
40. White, H. D., Belknap, B., and Webb, M. R. (1997) *Biochemistry* **36,** 11828–11836
41. De La Cruz, E. M., Ostap, E. M., and Sweeney, H. L. (2001) *J. Biol. Chem.* **276,** 32373–32381
42. Robblee, J. P., Olivares, A. O., and De La Cruz, E. M. (2004) *J. Biol. Chem.* **279,**

38608–38617
43. Kovacs, M., Wang, F., Hu, A., Zhang, Y., and Sellers, J. R. (2003) *J. Biol. Chem.* **278,** 38132–38140
44. Malnasi-Csizmadia, A., Pearson, D. S., Kovacs, M., Woolley, R. J., Geeves, M. A., and Bagshaw, C. R. (2001) *Biochemistry* **40,** 12727–12737
45. Urbanke, C., and Wray, J. (2001) *Biochem. J.* **358,** 165–173
46. Cuda, G., Pate, E., Cooke, R., and Sellers, J. R. (1997) *Biophys. J.* **72,** 1767–1779
47. Baker, J. E., Krementsova, E. B., Kennedy, G. G., Armstrong, A., Trybus, K. M., and Warshaw, D. M. (2004) *Proc. Natl. Acad. Sci. U. S. A.* **101,** 5542–5546
48. Rosenfeld, S. S., and Sweeney, H. L. (2004) *J. Biol. Chem.* **279,** 40100–40111